Higher-Order Spectral Analysis of a Nonlinear Pitch and Plunge Apparatus

Walter A. Silva*
NASA Langley Research Center, Hampton, Virginia, 23681
Thomas W. Strganac†
Texas A&M University, College Station, Texas
Muhammad R. Hajj‡
Virginia Polytechnic Institute and State University, Blacksburg, Virginia

Simulated aeroelastic responses of a nonlinear pitch and plunge apparatus are analyzed using various statistical signal processing techniques including higher-order spectral methods. A MATLAB version of the Nonlinear Aeroelastic Testbed Apparatus (NATA) at the Texas A&M University is used to generate various aeroelastic response data including limit cycle oscillations (LCO). Traditional and higher-order spectral (HOS) methods are applied to the simulated aeroelastic responses. Higher-order spectral methods are used to identify critical signatures that indicate the transition from linear to nonlinear (LCO) aeroelastic behavior.

Introduction

The study of nonlinear aeroelastic phenomena, in particular that of limit cycle oscillations (LCO), has become an important field of study in recent years.[1] A major motivating factor for this increased interest is the fact that several operational aircraft continue to experience LCO within their flight envelope, often leading to a flight restriction or performance degradation.[2,3] Several researchers have been using the Nonlinear Aeroelastic Testbed Apparatus (NATA) at Texas A&M University's Low-Speed Wind Tunnel to investigate fundamental aspects of LCO behavior.[4–9]

Recently, higher-order spectral methods have been applied to experimental flutter measurements from wind-tunnel data[10] and flight test data.[11] Analyses using higher-order spectral methods are proving beneficial to improved understanding of nonlinear aeroelastic phenomena. Higher-order spectral methods enable the visualization of the transfer of energy from one frequency to another, a hallmark of nonlinear phenomena that is not visible using traditional spectral methods.

The paper is organized as follows. A detailed description of the NATA and its MATLAB model are provided, including the equations of motion that define the dynamics of the system. A description of higher-order spectral (HOS) methods is provided, including an illustrative example. Simulated data generated using a variety of control surface inputs are then analyzed using traditional and HOS methods. The issue of the Gaussianess of an input/output combination for identifying regions of linear and nonlinear behavior is presented and applied.

Nonlinear Aeroelastic Testbed Apparatus (NATA)

The NATA in the Texas A&M University's 2 ft. x 3 ft. Low Speed Wind Tunnel is used to generate free and controlled, linear and nonlinear aeroelastic transients at various conditions. Based on a simple

*Senior Research Scientist, Aeroelasticity Branch, AIAA Associate Fellow.
†Associate Professor, Department of Aerospace Engineering, AIAA Associate Fellow.
‡Professor, Engineering Science and Mechanics.

two-degree-of-freedom concept with structurally nonlinear components, a rigid wing mounted on the NATA can exhibit nonlinear aeroelastic behavior, including LCO phenomena. The pitch and plunge motions of the NATA are enabled by springs that can be tuned to a wide variety of nonlinear stiffness characteristics. The NATA is shown in figure 1.

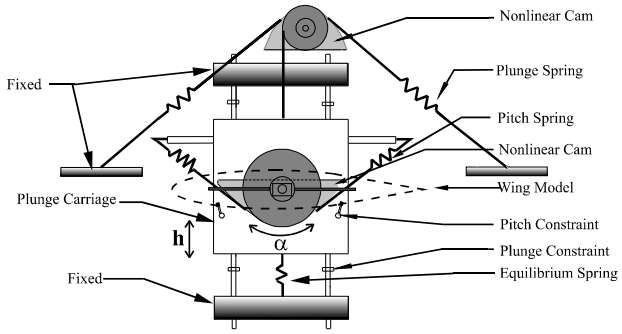

Figure 1. Schematic of the Nonlinear Aeroelastic Testbed Apparatus (NATA).

A rigid wing attached to the NATA, as it would be mounted in the Low Speed Wind Tunnel, is shown in figure 2. The nonlinear structural response is governed by a pair of cams that can be tuned to model various types of polynomial stiffness functions. Additional details regarding the NATA are available in the references.[4–8]

Analytical Model of NATA

A MATLAB model of the NATA/rigid wing system was generated and is briefly discussed in this section. The equations of motion for the system are presented as Eq. 1

$$\begin{bmatrix} m_T & m_w x_\alpha b \\ m_w x_\alpha b & I_\alpha \end{bmatrix} \begin{Bmatrix} \ddot{h} \\ \ddot{\alpha} \end{Bmatrix} + \begin{bmatrix} c_h & 0 \\ 0 & c_\alpha \end{bmatrix} \begin{Bmatrix} \dot{h} \\ \dot{\alpha} \end{Bmatrix} + \begin{bmatrix} k_h & 0 \\ 0 & k_\alpha(\alpha) \end{bmatrix} \begin{Bmatrix} h \\ \alpha \end{Bmatrix} = \begin{Bmatrix} -L \\ M \end{Bmatrix} \tag{1}$$

where

m_T total mass (wing and NATA)
m_w mass of the wing
x_α static unbalance

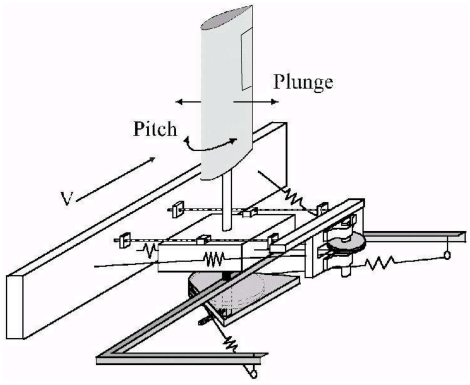

Figure 2. Schematic of the Nonlinear Aeroelastic Testbed Apparatus (NATA) with rigid airfoil and control surface.

b semichord
I_α mass moment of inertia about the elastic axis
h plunge degree of freedom
α pitch degree of freedom
c_h plunge damping coefficient
c_α pitch damping coefficient
k_h plunge stiffness coefficient
k_α pitch stiffness coefficient
L lift
M moment

The lift (L) and moment (M) on the right-hand side of Eq. 1 are defined using quasi-steady aerodynamics as presented in Eq. 2 and Eq. 3.

$$L = \rho U^2 b c_{l\alpha} \left(\alpha + \frac{\dot{h}}{U} + \left(\frac{1}{2} - a \right) b \frac{\dot{\alpha}}{U} \right) + \rho U^2 b c_{l\beta} \beta \tag{2}$$

$$M = \rho U^2 b^2 c_{m\alpha} \left(\alpha + \frac{\dot{h}}{U} + \left(\frac{1}{2} - a \right) b \frac{\dot{\alpha}}{U} \right) + \rho U^2 b^2 c_{m\beta} \beta \tag{3}$$

where

ρ density
U freestream velocity
$c_{l\alpha}$ lift due to angle of attack
$c_{l\beta}$ lift due to control surface deflection
β control surface deflection
$c_{m\alpha}$ moment due to angle of attack
$c_{m\beta}$ moment due to control surface deflection

Higher-Order Spectra

The primary benefit of higher-order spectra (HOS), also known as higher-order frequency response functions, is that they provide information regarding the interaction of frequencies due to a nonlinear process. For example, bispectra have been used in the study of grid-generated turbulence to identify the nonlinear exchange of energy from one frequency to another (related to the turbulent cascade phenomenon). Traditional, or standard, concepts, by definition, cannot provide this type of information. In addition, higher-order spectra are the frequency-domain version of the Volterra series. For details regarding this relationship, the reader is referred to the recent article by Silva.[12] Some very interesting and fundamental applications using the frequency-domain Volterra theory[13,14] and experimental applications of Volterra methods[15,16] are providing new "windows" on the world of nonlinear aeroelasticity.

In the recent work by Hajj and Silva,[17,18] the aerodynamic and structural aspects of the flutter phenomenon of a wind-tunnel model are determined via a frequency domain analysis based on a hierarchy of spectral moments. The power spectrum is used to determine the distribution of power among the frequency components in the pressure, strain and acceleration data. The cross-power spectrum, linear coherence, and phase relation of the same frequency components between different signals are used to characterize the bending and torsion characteristics of the model. The nonlinear aspects of the aerodynamic loading are determined from estimates of higher-order spectral moments, namely, the auto- and cross-bispectrum.

For a discrete, stationary, real-valued, zero-mean process, the auto-bispectrum is estimated as[19]

$$\hat{B}_{xxx}[l_1, l_2] = \frac{1}{M} \sum_{k=1}^{M} X_T^{(k)}[l_1 + l_2] X_T^{*(k)}[l_1] X_T^{*(k)}[l_2] \tag{4}$$

where $X_T^{(k)}[l]$ is the Discrete Fourier Transform of the k^{th} ensemble of the time series $x(t)$ taken over a time, T, and M is the number of these ensembles. The auto-bispectrum of a signal is a two-dimensional function of frequency and is generally complex-valued. In averaging over many ensembles, the magnitude of the auto-bispectrum will be determined by the presence (or absence) of a phase relationship among sets of the frequency components at l_1, l_2, and $l_1 + l_2$. If there is a random phase relationship among these three components, the auto-bispectrum will average to a very small value. Should a phase relationship exist among these frequency components, the corresponding auto-bispectrum will have a large magnitude.[20] Because a quadratic nonlinear interaction between two frequency components, l_1 and l_2, yields a phase relation between them and their summed component, $l_1 + l_2$, the auto-bispectrum can be used to detect a quadratic coupling or interaction among different frequency components of a signal. The level of such coupling in a signal can then be associated with a normalized quantity of the auto-bispectrum, called the auto-bicoherence, and defined as

$$b^2_{xxx}[l_1, l_2] = \frac{\left|\hat{B}_{xxx}[l_1, l_2]\right|^2}{\frac{1}{M}\sum_{k=1}^{M}\left|X_T^{(k)}[l_1] X_T^{(k)}[l_2]\right|^2 \frac{1}{M}\sum_{k=1}^{M}\left|X_T^{(k)}[l_1+l_2]\right|^2} \tag{5}$$

By the Schwarz inequality, the value of $b^2_{xxx}[l_1, l_2]$ varies between zero and one. If no phase relationship exists among the frequency components at l_1, l_2, and $l_1 + l_2$, the value of the auto-bicoherence will be at or near zero (due to averaging effects). If a phase relationship does exist among the frequency components at l_1, l_2, and $l_1 + l_2$, then the value of the auto-bicoherence will be near unity. Values of the auto-bicoherence between zero and one indicate partial quadratic coupling.

For systems where multiple signals are considered, detection of nonlinearities can be achieved by using the cross-spectral moments. For two signals $x(t)$ and $y(t)$, their cross-bispectrum is estimated as

$$\hat{B}_{yxx}[l_1, l_2] = \frac{1}{M} \sum_{k=1}^{M} Y_T^{(k)}[l_1 + l_2] X_T^{*(k)}[l_1] X_T^{*(k)}[l_2] \tag{6}$$

where $X_T^{(k)}[l]$ and $Y_T^{(k)}[l]$ are the Discrete Fourier Transforms of the k^{th} ensemble of the time series $x(t)$ and $y(t)$, respectively, over a time, T. The cross-bispectrum provides a measure of the nonlinear relationship among the frequency components at l_1 and l_2 in $x(t)$ and their summed frequency component, $l_1 + l_2$, in $y(t)$. Similar to the auto-bispectrum, the cross-bispectrum of signals $x(t)$ and $y(t)$ is a two-dimensional

function in frequency and is generally complex-valued. In averaging over many ensembles, the magnitude of the cross-bispectrum will also be determined by the presence, or absence, of a phase relationship among sets of the frequency components at l_1, l_2, and $l_1 + l_2$. If there is a random phase relationship among the three components, the cross-bispectrum will average to a very small value. Should a phase relationship exist among these frequency components, the corresponding cross-bispectral value will have a large magnitude. The cross-bispectrum is thus able to detect nonlinear phase coupling among different frequency components in two signals because of its phase-preserving effect.

Similar to defining the auto-bicoherence, one can define a normalized cross-bispectrum to quantify the level of quadratic coupling in two signals. This normalized value is called the cross-bicoherence and is defined as

$$b^2_{yxx}[l_1, l_2] = \frac{\left|\hat{B}_{yxx}[l_1, l_2]\right|^2}{\frac{1}{M}\sum_{k=1}^{M}\left|X_T^{(k)}[l_1]X_T^{(k)}[l_2]\right|^2 \frac{1}{M}\sum_{k=1}^{M}\left|Y_T^{(k)}[l_1+l_2]\right|^2} \tag{7}$$

If no phase relationship exists among the frequency components at l_1, l_2 in $x(t)$ and the frequency component at $l_1 + l_2$ in $y(t)$, the value of the cross-bicoherence will be at or near zero. If a phase relationship does exist among these frequency components, the value of the cross-bicoherence will be near unity. Values of cross-bicoherence between zero and one indicate partial quadratic coupling. A digital procedure for computing the auto and cross-bicoherence is given by Kim and Powers[19] and is summarized by Hajj et al.[21]

An important property of HOS functions involves the Gaussianess of a signal. The auto-bicoherence of a Gaussian signal is identically zero. This is an important theoretical result that is described in the literature. In addition, it is well-known that if a Gaussian signal is input to a linear system, then the output will be Gaussian as well. Therefore, computation of the auto-bicoherence for a Gaussian output will yield a value at or near zero, indicative of a linear process. If a Gaussian signal is applied to a nonlinear system, the output will be non-Gaussian. As a result, the auto-bicoherence for the output of the nonlinear system will yield a non-zero value. This characteristic of HOS methods is exploited for the present application to identify regions where the behavior is transitioning from linear to nonlinear dynamics.

Using a linear (Eq. 8) and a nonlinear differential equation (van der Pol oscillator, Eq. 9), the effect of nonlinear processes on input Gaussian distributions can be demonstrated. A Gaussian signal is input to the linear and nonlinear differential equations. The histogram of the response for each system (linear and nonlinear) to the Gaussian input signal is presented in the following figures.

Presented in Figure 3 are the input and output histograms for the linear system. As can be seen, the linear system preserves the Gaussianess of the input signal. Presented in Figure 4 are the input and output histograms for the nonlinear system. For the nonlinear case, the Gaussianess of the input signal has not been preserved and has, instead, been transformed into a non-Gaussian distribution radically different from the input distribution. This is a well-known characteristic of nonlinear systems. It is worthwhile to mention that the response of the van der Pol oscillator (the nonlinear ODE) is a limit cycle oscillation (LCO). It appears that the distribution for other LCO phenomena may have a similar structure.

HOS methods are very sensitive to variations in Gaussianess and, as will be shown, are valuable in identifying deviations from Gaussian behavior. Deviations from Gaussian behavior, as shown above, indicate the existence of a nonlinear process.

$$\dot{y_1} = y_2, \dot{y_2} = -y_2 - y_1 + input \tag{8}$$

$$\dot{y_1} = y_2, \dot{y_2} = -\mu(1 - y_1)^2 y_2 - y_1 + input \tag{9}$$

Example 2

A second example is now presented in order to explain some of the concepts associated with HOS. The example[22] consists of a linear (y) and a nonlinear (z) time series, both containing Gaussian noise (d). The equations for these time series are

$$x(k) = \sin(2\pi(f_1)k + \frac{\pi}{3}) + \sin(2\pi(f_2)k + \frac{\pi}{8}) \tag{10}$$

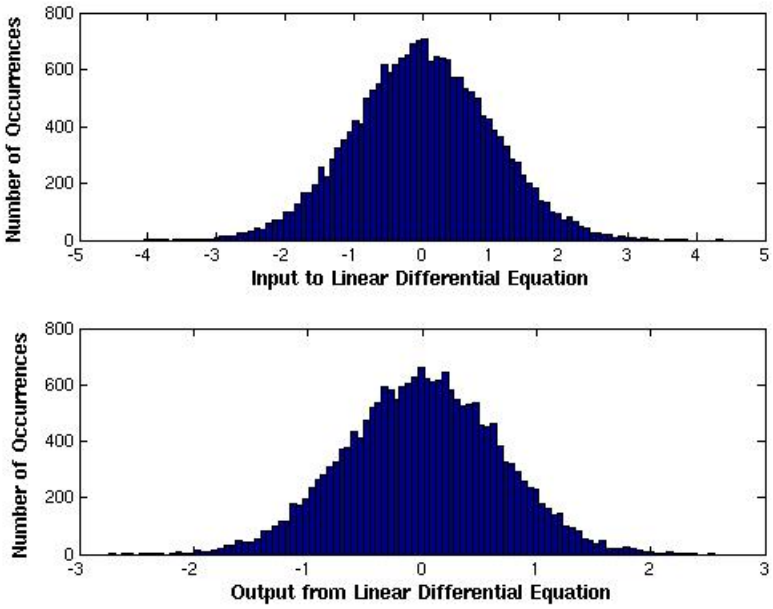

Figure 3. Histograms of the input and output for the linear system due to a Gaussian input.

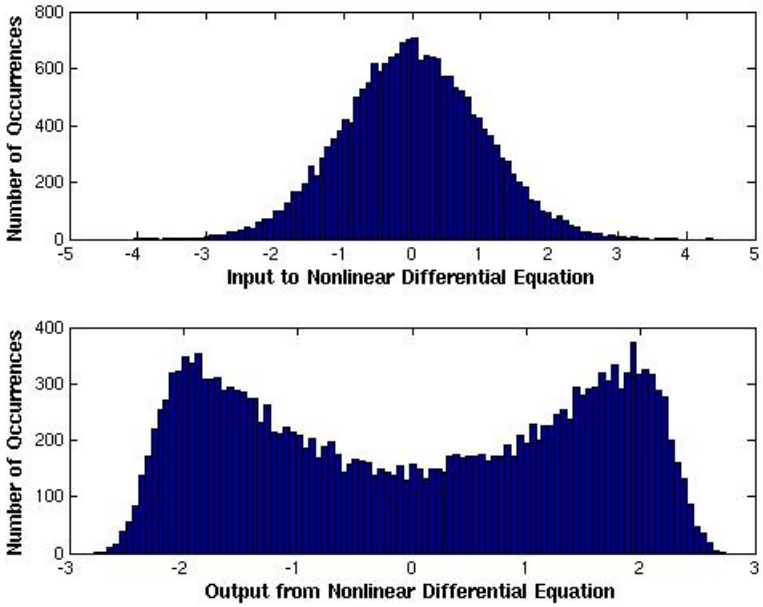

Figure 4. Histograms of the input and output for the nonlinear system due to a Gaussian input.

$$y(k) = x(k) + d(k) \tag{11}$$

$$z(k) = x(k) + 0.05x^2(k) + d(k) \tag{12}$$

where $f_1 = 0.12$ Hz and $f_2 = 0.30$ Hz.

Figures 5 and 6 each contain the time series and the associated magnitude of the Fourier transforms for the linear and nonlinear time series, respectively. The dominant frequencies (in this case 0.12 and 0.30 Hz) are clearly visible in both figures. The frequency content for the nonlinear time series indicates the existence of additional frequencies. The nature of these frequencies, whether or not these frequencies are random or the result of a nonlinear coupling process, cannot be discerned from this analysis.

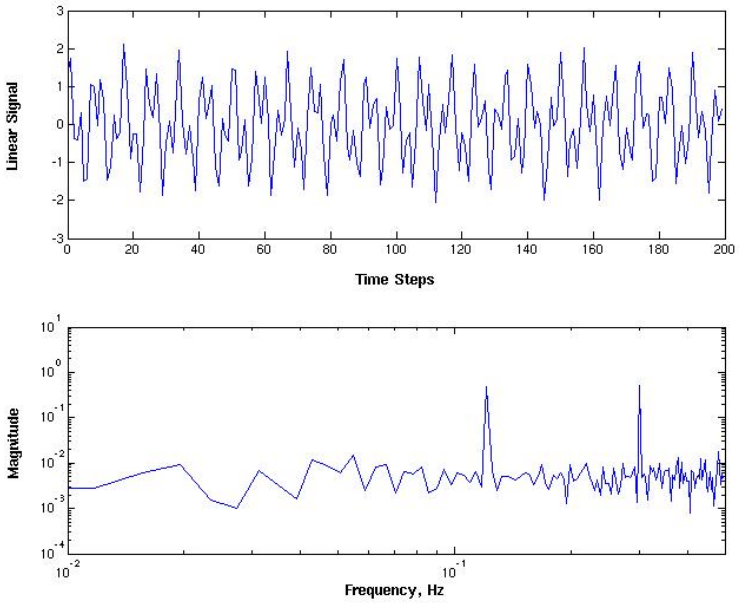

Figure 5. Linear time series and magnitude of frequency response.

The power spectral densities (PSD) for the linear and nonlinear time series are presented as Figure 7. Here again, the existence of additional frequencies in the PSD of the nonlinear time series (as compared to the linear time series) is obvious. However, the PSD information cannot be used to discern if these additional frequencies are random or the result of a nonlinear coupling process.

In order to determine if these additional frequencies are random or the result of a nonlinear coupling process, the HOS for these time series must be computed. The magnitude of the auto-bicoherence for the linear time series, y, is presented as Figure 8. The two frequency axes correspond to the two frequency indices in Eq. 5. If a significant peak is observed, this implies that the sum of those two frequencies is the result of a quadratic (nonlinear) coupling. It can be seen that the magnitude of the auto-bicoherence for the linear time series is quite low in value (compared to unity) and that there exist no dominant peaks that would be indicative of a nonlinear coupling.

The magnitude of the auto-bicoherence for the nonlinear time series is presented as Figure 9. In contrast to the auto-bicoherence for the linear time series, the auto-bicoherence for the nonlinear time series has several peaks at or close to unity, indicative of nonlinear (quadratic) coupling at the x- and y-axis frequencies indicated.

Typically, to enhance visualization and interpretation of the auto- or cross-bicoherence , contour plots are viewed. The contour plot for Figure 9 is presented as Figure 10. The contour plot presents the frequencies that have coupled quadratically to generate the new frequencies that were visible in the PSD. In addition, the symmetry associated with the computation of the auto-bicoherence, in this case, is also evident in the

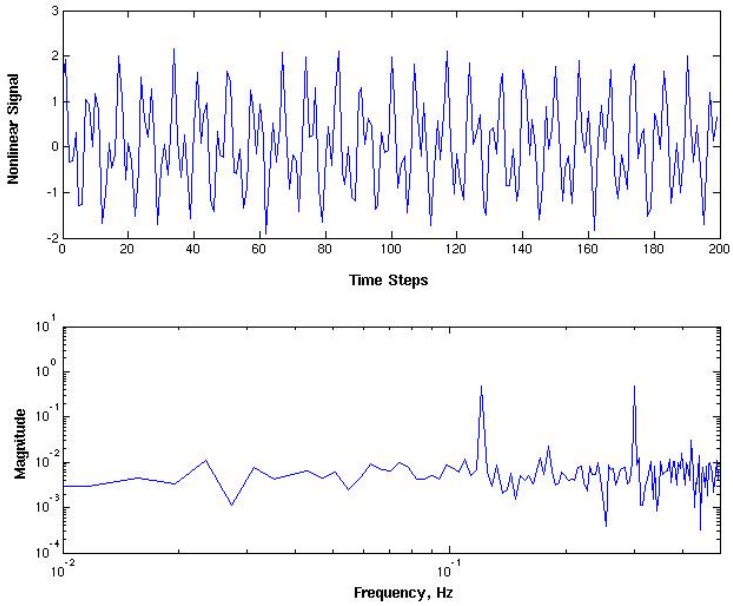

Figure 6. Nonlinear time series and magnitude of frequency response.

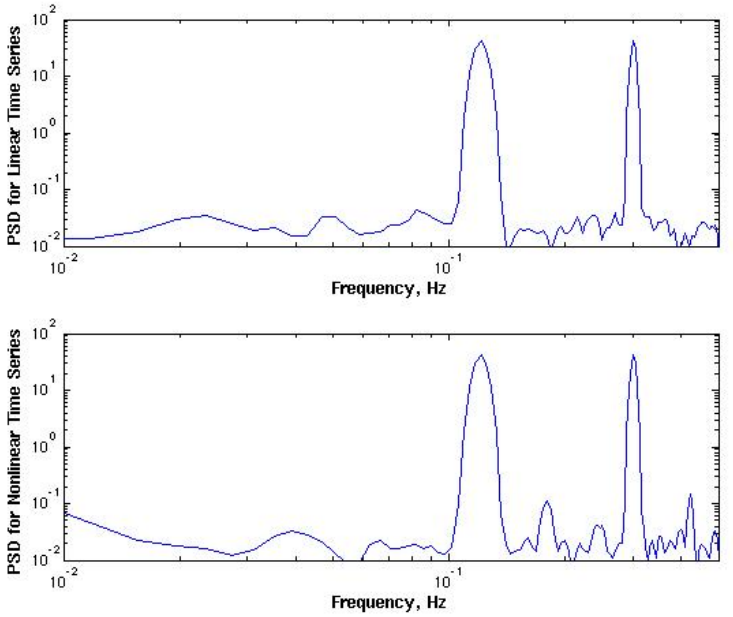

Figure 7. Power spectral density (PSD) functions for linear and nonlinear time series.

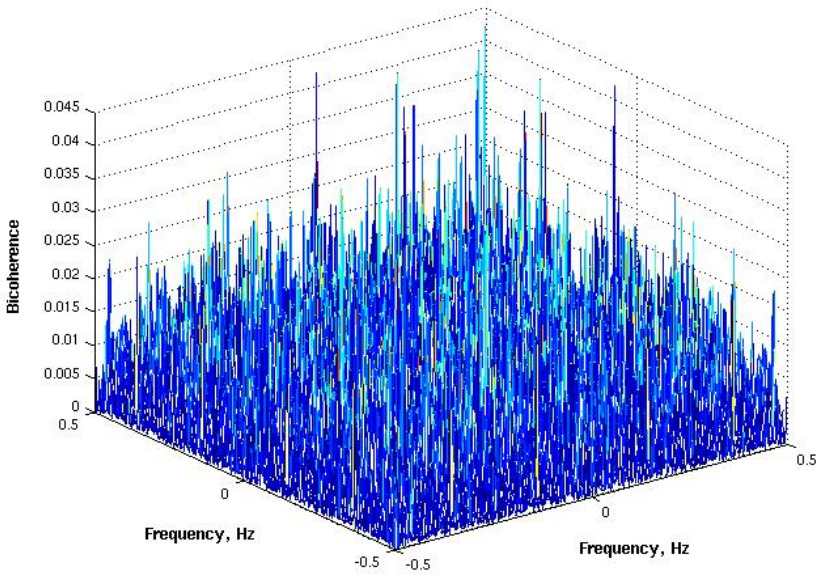

Figure 8. Auto-bicoherence for the linear time series.

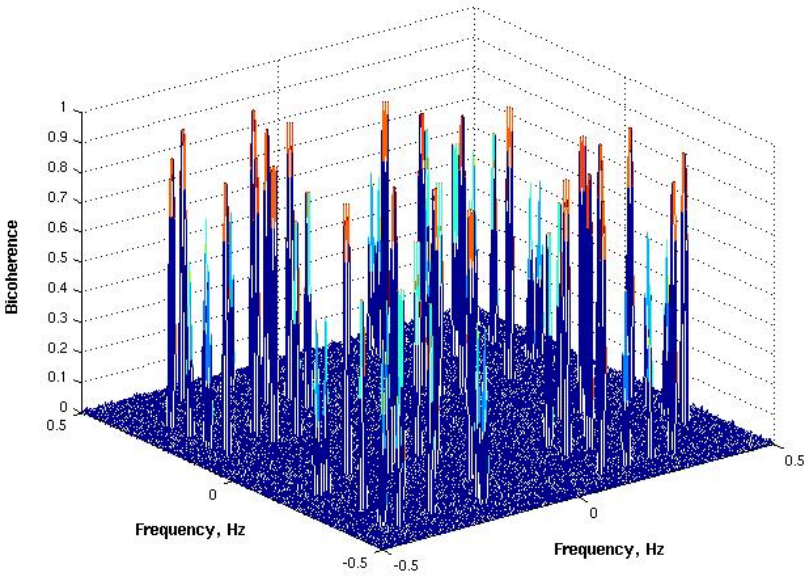

Figure 9. Auto-bicoherence for the nonlinear time series.

contour plot. The bicoherence basically computes the correlation between two frequencies and the sum of those two frequencies. For example, the magnitude of the auto-bicoherence when the first frequency (x-axis) is 2 Hz and the second frequency (y-axis) is 5 Hz will be the same as the magnitude of the auto-bicoherence when the first frequency is 5 Hz and the second frequency is 2 Hz since their sum is the same.

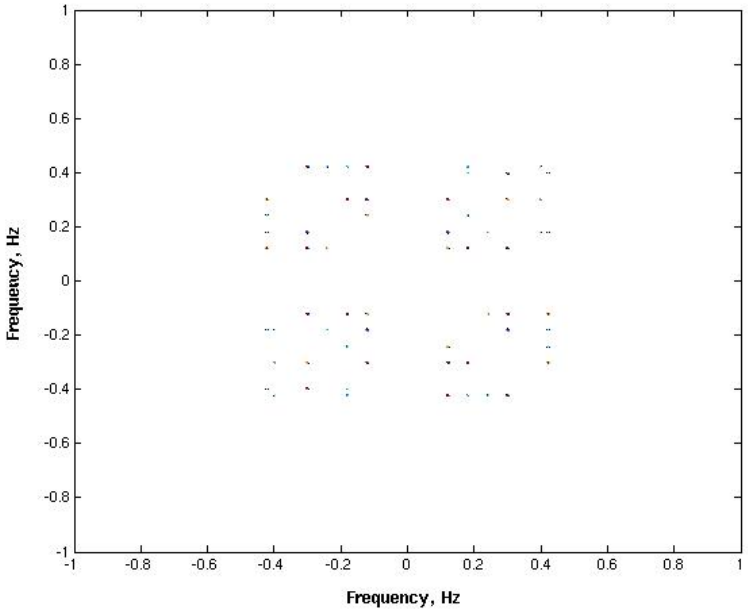

Figure 10. Contour plot of the auto-bicoherence for the nonlinear time series.

This symmetry is presented in Figure 11. As Figure 11 indicates, knowledge of Region I (two such regions in the first quadrant) and Region II (two such regions in the fourth quadrant) is sufficient to completely define the remainder of the quadrants due to symmetry considerations. Regions I and II indicate that the original frequencies have been quadratically-coupled, resulting in new frequencies that are the sum (positive and negative) of the original frequencies. The new frequencies include 0.18, 0.24, and 0.42. The limitation of Region I to the triangle shown is due to the fact that the summation of two frequencies cannot exceed the Nyquist frequency (0.5, in this case). Therefore, the combination of the second frequency (0.30 Hz) with itself is not included since 0.60 Hz would be greater than the Nyquist frequency.

For subsequent results, although the auto-bicoherence is computed for all frequencies (positive and negative), Region I in the first quadrant will be of primary interest for the sake of simplicity. This will be sufficient to demonstrate the applicability and value of HOS methods to aeroelastic data.

Results

In this section, aeroelastic transients that range from a stable response to an LCO response, generated in MATLAB using the analytical model of the NATA, are presented. Then, in order to investigate the level of nonlinearity for each transient, Gaussian inputs will be applied to the system via the control surface. The output responses will be analyzed for their level of Gaussianity. Deviations from a Gaussian distribution can be interpreted as deviations from linear behavior. The auto-bicoherence is also presented to demonstrate the ability of HOS methods to discern Gaussianess from non-Gaussianess. For simplicity, the results presented are limited to the pitch motion.

Figure 12 presents the aeroelastic transient in pitch for a condition where a stable aeroelastic response is generated at a small velocity (U=5 m/sec) with small initial conditions as perturbations and no control surface input. The aeroelastic transient is clearly stable and the frequencies of the system are evident in the plot of the magnitude of the frequency response function of the pitch motion.

Figure 13 presents the aeroelastic transient in pitch for a condition where an LCO has been reached at a

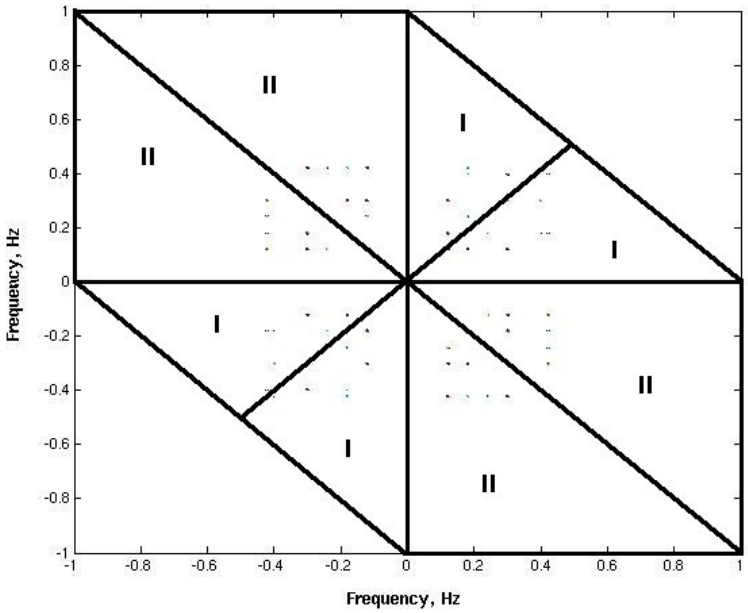

Figure 11. Contour plot of the auto-bicoherence for the nonlinear time series with symmetry regions identified.

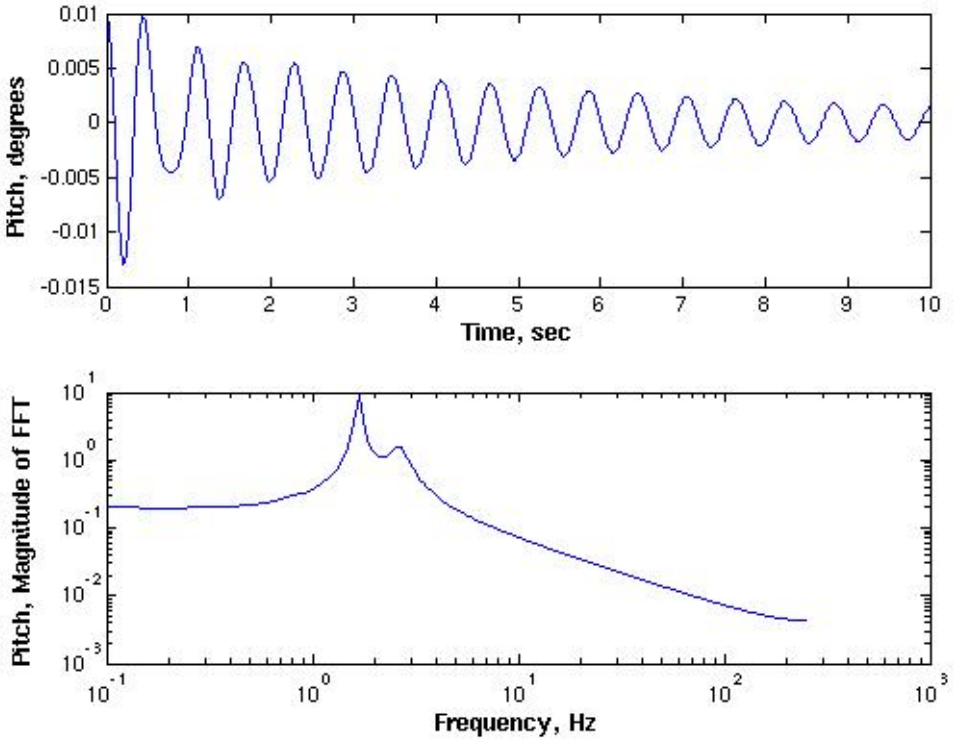

Figure 12. Stable aeroelastic response in pitch at U=5 m/sec: Time domain and frequency domain.

velocity of U=20 m/sec. The frequency content is exhibiting greater complexity than the previous aeroelastic transient.

To determine the level of nonlinearity that may be present starting from the stable transient (U=5 m/sec) all the way to the LCO transient (U=20 m/sec), a Gaussian input is applied via the control surface and the resulting nature of the output transient (Gaussian or non-Gaussian) is determined. This approach serves to demonstrate the sensitivity of HOS methods to non-Gaussian signals.

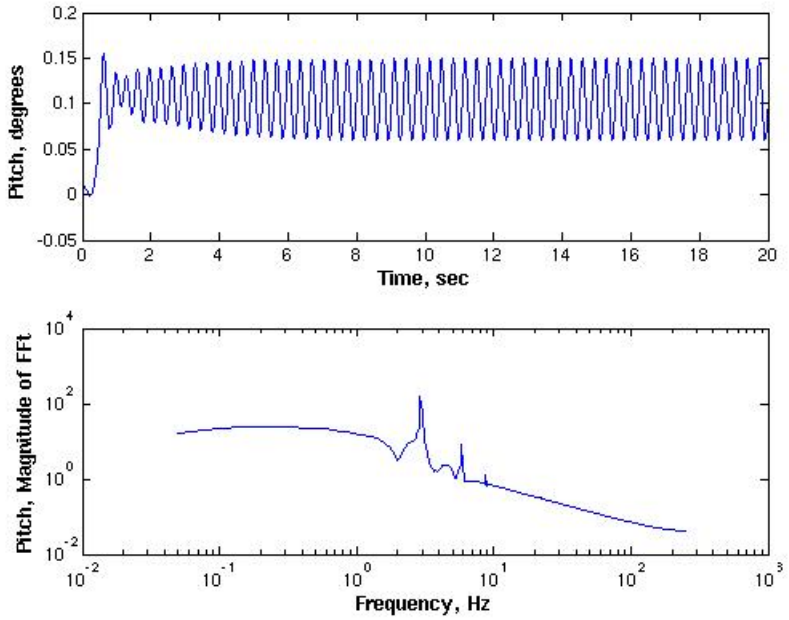

Figure 13. Limit cycle oscillation (LCO) aeroelastic response in pitch at U=20 m/sec: Time and frequency domain.

A Gaussian input is generated and applied to the aeroelastic system via the control surface. The histogram of the input is presented as Figure 14, where the Gaussian nature of the signal is evident. The auto-bicoherence for the Gaussian input is presented as Figure 15. The small values of the auto-bicoherence for the Gaussian input are as expected for a signal with a Gaussian distribution.

The resultant aeroelastic response (at U=5 m/sec) and the corresponding magnitude of the frequency response are presented in Figure 16. The effect of the Gaussian input is evident in the transient as well as the frequency content when Figure 16 is compared with Figure 12. However, neither of these two functions can be used to indicate the presence or level of any nonlinear interactions. The histogram of the output response (pitch, in this case) is presented as Figure .

The histogram for the output response indicates a noticeable deviation from the theoretical Gaussian distribution , indicating that the Gaussian input has been processed through some level of nonlinear interactions.

The auto-bicoherence for this aeroelastic response, presented as Figure 18, confirms the existence of nonlinear coupling at frequencies close to the LCO frequency ($\tilde{3}$ Hz).

The velocity is increased to U=10 m/sec and the same Gaussian input is applied. The aeroelastic response, along with the magnitude of the frequency response, is presented in Figure 19.

Once again, the information presented in Figure 19 cannot be used to discern if any nonlinear interactions are taking place at this condition. However, the histogram of the output, presented as Figure 20, indicates an increased level of deviation from Gaussianess.

The auto-bicoherence for this condition is presented as Figure 21, with increasing levels of nonlinear interaction near the frequency of the LCO. The important point to be made is that both, the histograms and the auto-bicoherence, are indicating the presence of nonlinear phenomena prior to the visible onset of the LCO at U=20 m/sec.

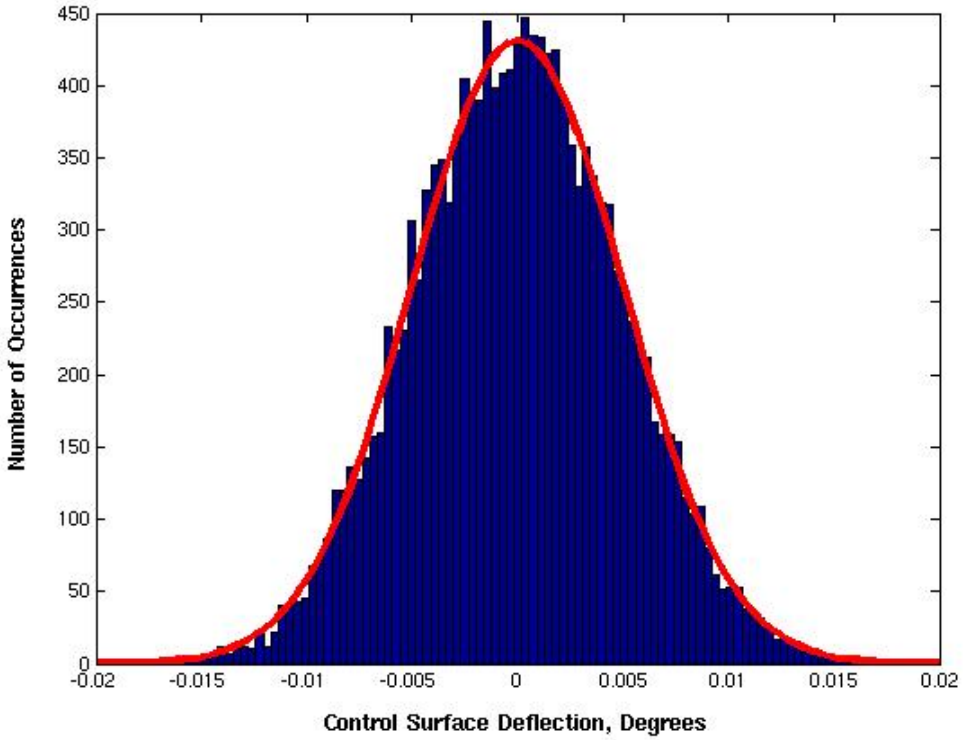

Figure 14. Histogram of the Gaussian input and theoretical Gaussian distribution (red).

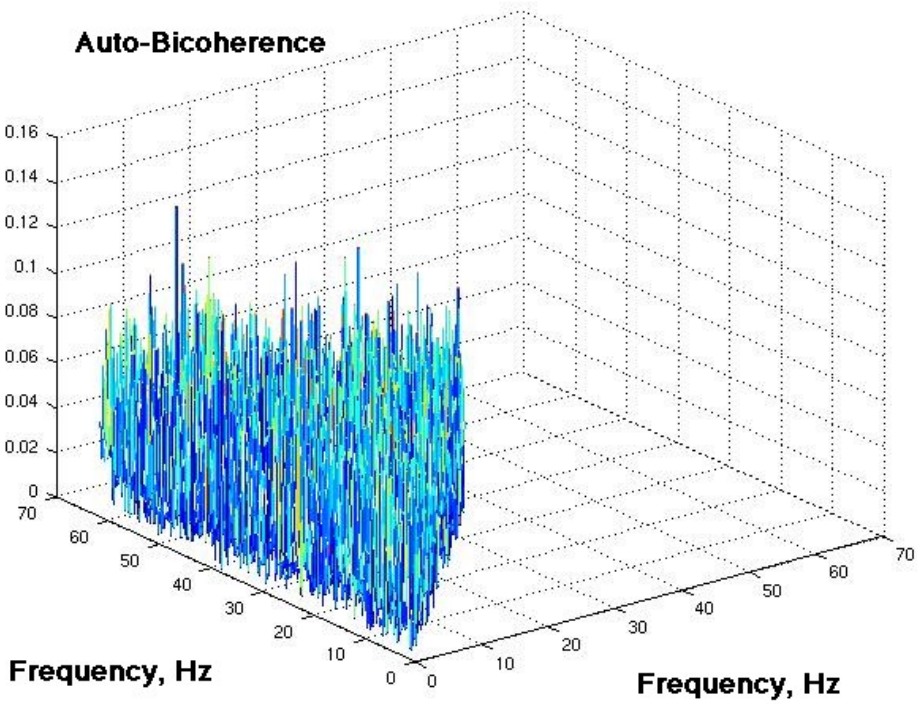

Figure 15. Auto-bicoherence of the Gaussian control surface input.

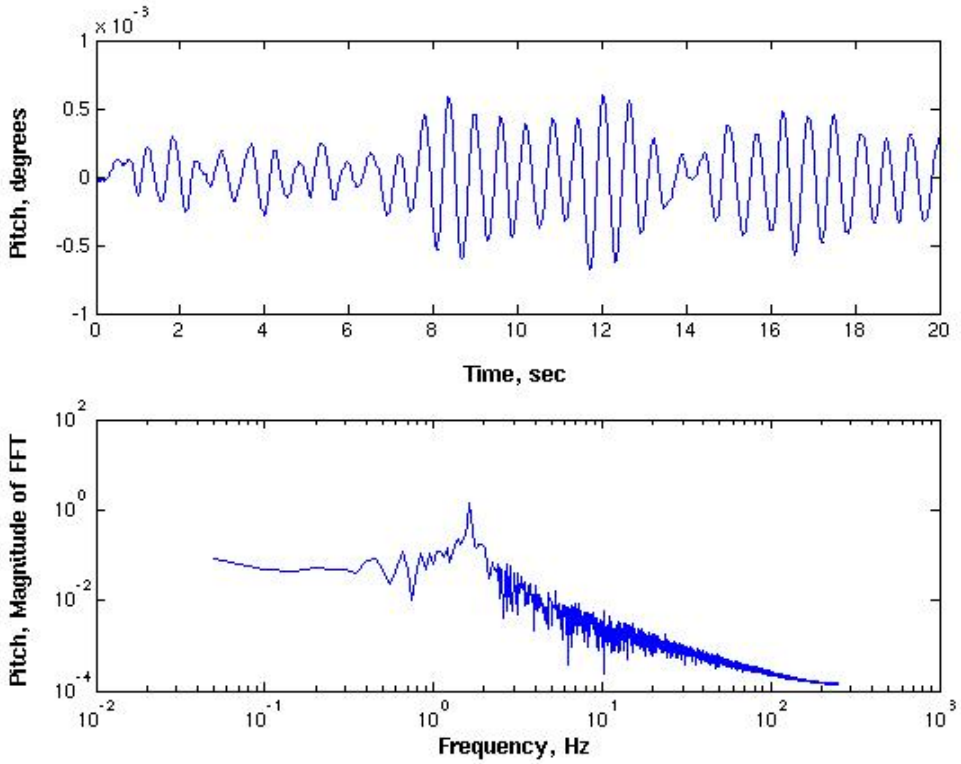

Figure 16. Stable aeroelastic response in pitch at U=5 m/sec with Gaussian control surface input: Time and frequency domain.

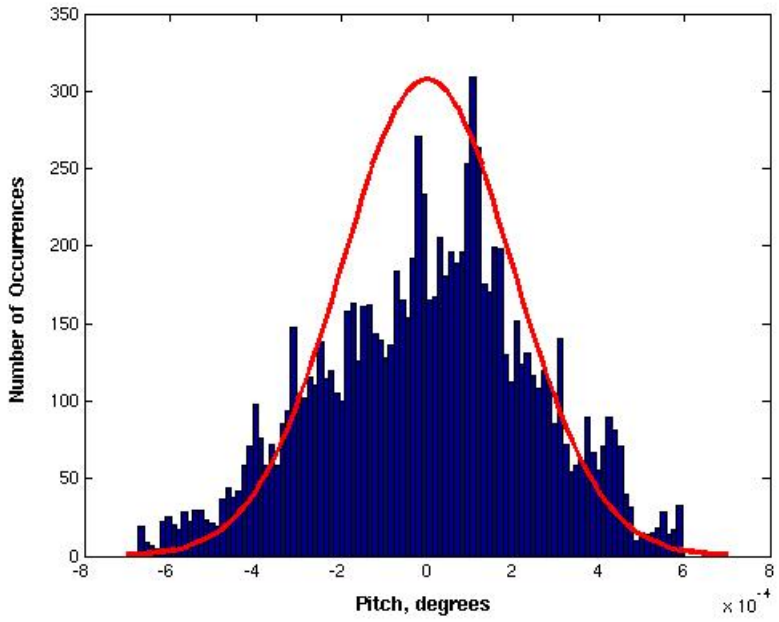

Figure 17. Histogram of stable aeroelastic response in pitch at U=5 m/sec due to Gaussian control surface input.

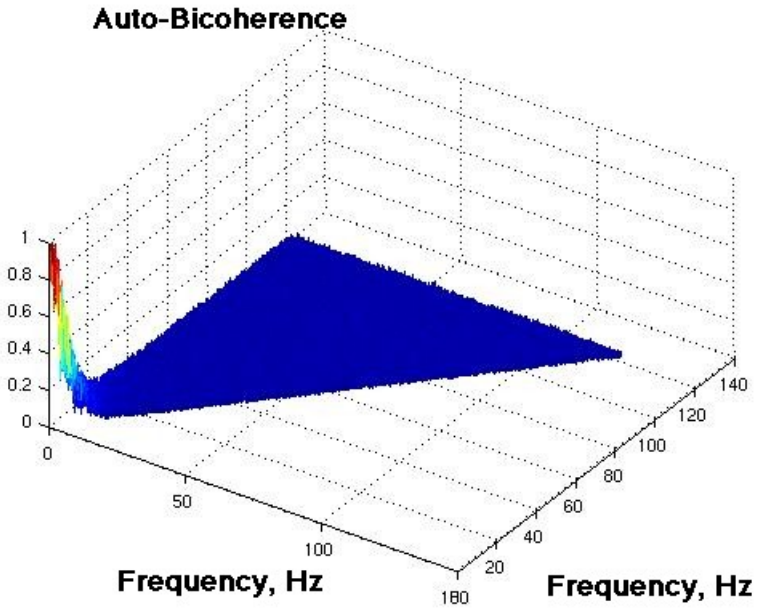

Figure 18. Auto-bicoherence of stable aeroelastic response in pitch at U=5 m/sec due to Gaussian control surface input.

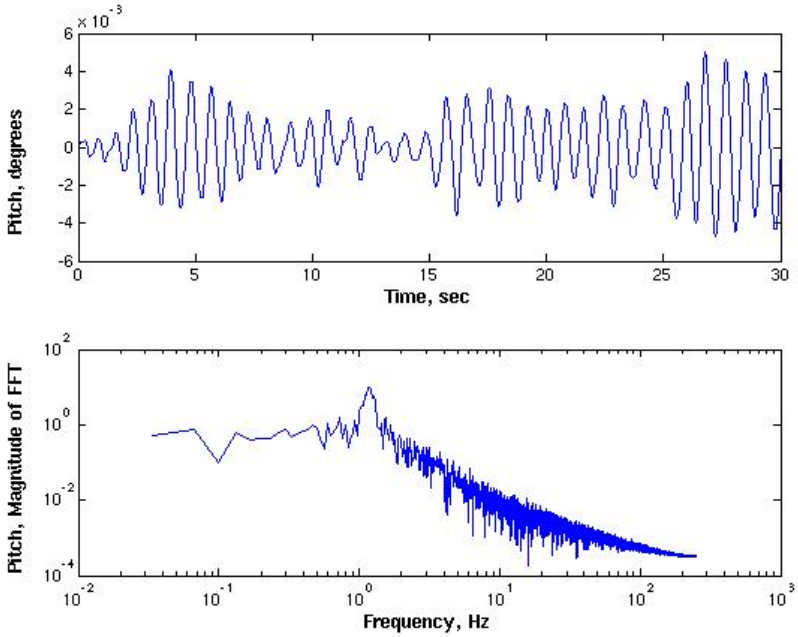

Figure 19. Stable aeroelastic response in pitch at U=10 m/sec with Gaussian control surface input: Time and frequency domain.

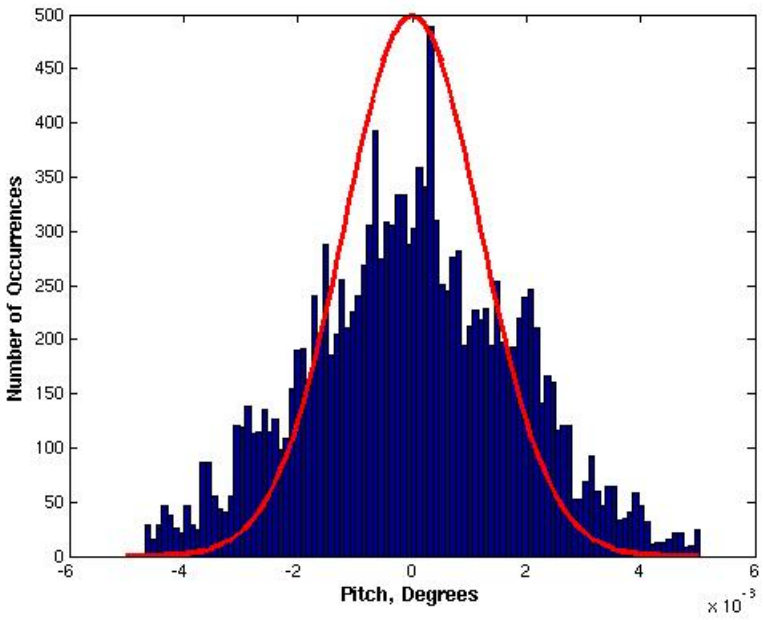

Figure 20. Histogram of stable aeroelastic response in pitch at U=10 m/sec due to Gaussian control surface input.

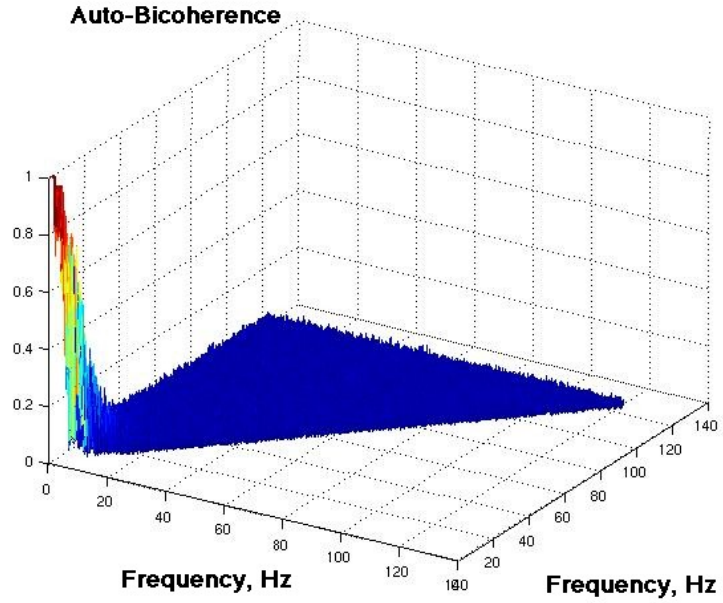

Figure 21. Auto-bicoherence of stable aeroelastic response in pitch at U=10 m/sec due to Gaussian control surface input.

The same Gaussian control surface input was applied for the U=20 m/sec condition at which LCO is encountered. The resulting LCO aeroelastic transient and the corresponding magnitude of the frequency response in pitch for that conditions is presented as Figure 22. The histogram of the pitch response is presented as Figure 23, where the deviation from Gaussianess is obvious. The resulting histogram of the LCO pitch response is clearly non-Gaussian with a bi-modal character. Figure 24 presents the corresponding aut-bicoherence for this condition. The auto-bicoherence for this LCO condition captures the nonlinear interactions that occur in the vicinity of the LCO frequency with greater resolution than the previous conditions.

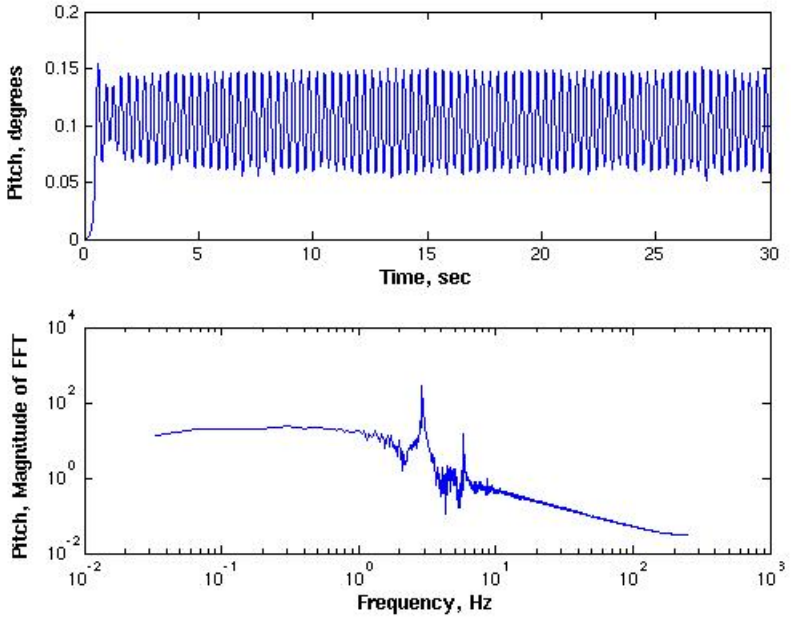

Figure 22. LCO aeroelastic response in pitch at U=20 m/sec with Gaussian control surface input: Time and frequency domain.

Therefore, using this type of information (input/output histograms and auto-bicoherence) may enable the identification of precipitous nonlinear behavior prior to the actual onset during wind-tunnel or flight testing. This capability would provide greater insight into the testing process as well as enhanced insight regarding the nature of the nonlinear aeroelastic response.

Conclusion

Simulated responses from a MATLAB model of the Texas A&M University's Nonlinear Aeroelastic Testbed Apparatus (NATA) with a rigid wing were presented. Aeroelastic transients generated included stable aeroelastic responses as well as nonlinear responses, or limit cycle oscillations (LCO). A Gaussian input was applied to the system via the control surface in order to determine the deviation from Gaussian behavior (i.e., deviation from linear behavior) of the aeroelastic system. Higher-order spectra were computed and served to indicate the existence of nonlinear interactions prior to the LCO event.

Acknowledgments

The first author would like to acknowledge NASA Langley's Office of Employee Development for support of this research effort via the Floyd L. Thompson Fellowship.

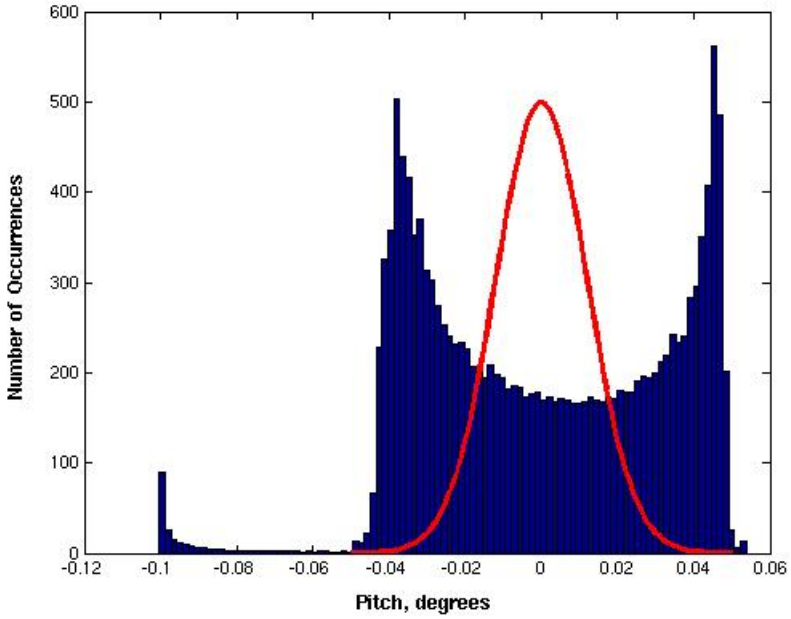

Figure 23. Histogram of stable aeroelastic response in pitch at U=10 m/sec due to Gaussian control surface input.

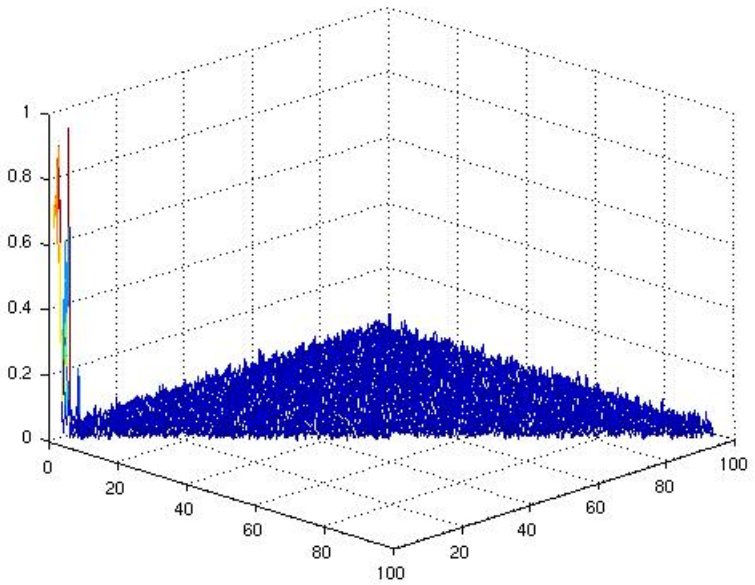

Figure 24. Auto-bicoherence of stable aeroelastic response in pitch at U=10 m/sec due to Gaussian control surface input.

References

[1]Dowell, E. H., Edwards, J. W., and Strganac, T., "Nonlinear Aeroelasticity," *Journal of Aircraft*, Vol. 40, Sept. 2003, pp. 857–874.

[2]Dunn, S. A., Farrell, P. A., Budd, P. J., Arms, P. B., Hardie, C. A., and Rendo, C. J., "F/A-18A Flight Flutter Testing-Limit Cycle Oscillation or Flutter?" *International Forum on Aeroelasticity and Structural Dynamics*, No. 00-2401, Madrid, Spain, June 2001.

[3]Denegri, C. M., "Limit Cycle Oscillation Flight Test Results of a Fighter with External Stores," *Journal of Aircraft*, Vol. 37, June 2001, pp. 761–769.

[4]O'Neill, T. G., "Experimental and Analytical Investigations of an Aeroelastic Structure with Continuous Nonlinear Stiffness," *PhD Thesis*, College Station, TX, May 1996.

[5]Block, J. J., "Active Control of an Aeroelastic Structure," *PhD Thesis*, College Station, TX, May 1996.

[6]Block, J. J. and Strganac, T. W., "Applied Active Control for a Nonlinear Aeroelastic Structure," *Journal of Guidance, Control, and Dynamics*, Vol. 21, 1998, pp. 838–845.

[7]Strganac, T. W., Ko, J., Thompson, D. E., and Kurdila, A. J., "Investigations of Limit Cycle Oscillations in Aeroelastic Systems," *International Forum on Aeroelasticity and Structural Dynamics*, jun 1999.

[8]Strganac, T. W., Ko, J., and Thompson, D. E., "Identification and Control of Limit Cycle Oscillations in Aeroelastic Systems," *Journal of Guidance, Control, and Dynamics*, Vol. 23, jun 2000, pp. 1127–1133.

[9]Thompson, D., "Nonlinear Analysis of Store-Induced Limit Cycle Oscillations," *PhD Thesis*, College Station, TX, Aug. 2001.

[10]Hajj, M. R. and Silva, W. A., "Nonlinear Flutter Aspects of the Flexible High-Speed Civil Transport Semispan Model," *Journal of Aircraft*, Vol. 41, 2004, pp. 1202–1208.

[11]Silva, W. A. and Dunn, S., "Higher-Order Spectral Analysis of F-18 Flight Flutter Data," *46th AIAA/ASME/ASCE/AHS/ASC Structures, Structural Dynamics, and Materials Conference*, No. 2005-2014, apr 2005.

[12]Silva, W. A., "Identification of Nonlinear Aeroelastic Systems Based on the Volterra Theory: Progress and Opportunities," *Journal of Nonlinear Dynamics*, Vol. 39, Jan. 2005.

[13]Marzocca, P., Librescu, L., and Silva, W. A., "Nonlinear Stability and Response of Lifting Surfaces via Volterra Series," *presented at the 20th International Congress of Theoretical and Applied Mechanics, Chicago, IL*, 27 August - 2 September 2000.

[14]Marzocca, P., Librescu, L., and Silva, W. A., "Volterra Series Approach for Nonlinear Aeroelastic Response of 2-D Lifting Surfaces," *presented at the 42nd Structures, Structural Dynamics, and Materials Conference, 16-19 April 2001, Seattle, WA*, 16-19 April 2001.

[15]Kurdila, A. J., Carrol, B., Nishida, T., and Sheplak, M., "Reduced-Order Modeling for Low Reynolds Number Flow Control," *SPIE Conference on Mathematics and Control in Smart Structures, Newport Beach, CA*, Vol. 3667, March 1999, pp. 68–79.

[16]Prazenica, R., Kurdila, A., and Silva, W. A., "Multiresolution Methods for Representation of Volterra Series and Dynamical Systems," AIAA Paper 2000-1754, April 2000.

[17]Hajj, M. R. and Silva, W. A., "Nonlinear Flutter Aspects of the Flexible HSCT Semispan Model," *Proceedings of the 44th Structures, Structural Dynamics and Materials Conference*, No. 2003-1515, Norfolk, VA, April 2003.

[18]Hajj, M. R. and Silva, W. A., "Nonlinear Flutter Aspects of the Flexible HSCT Semispan Model," *International Forum on Aeroelasticity and Structural Dynamics*, No. US-39, Amsterdam, The Netherlands, 4-6 June 2003.

[19]Kim, Y. C. and Powers, E. J., "Digital Bispectral Analysis and its Applications to Nonlinear Wave Interactions," *IEEE Transactions of Plasma Science*, Vol. PS-7, 1979, pp. 120–131.

[20]Hajj, M. R., Miksad, R. W., and Powers, E. J., "Fundamental Subharmonic Interaction: Effect of the Phase Relation," *Journal of Fluid Mechanics*, 1993.

[21]Hajj, M. R., Miksad, R. W., and Powers, E. J., "Perspective: Measurements and Analyses of Nonlinear Wave Interactions with Higher-Order Spectral Moments," *Journal of Fluid Engineering*, 1997.

[22]Choudhury, M. A. A. S., Shah, S. L., and Thornhill, N. F., "Detection and Diagnosis of System Nonlinearities Using Higher Order Statistics," *15th Triennial IFAC World Congress*, Barcelona, Spain, 2002.